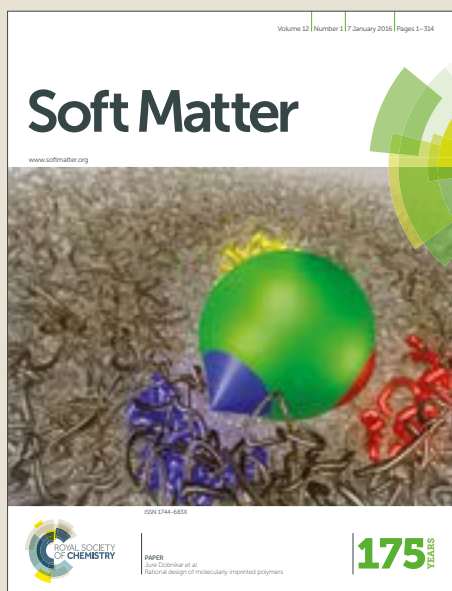


Soft Matter

Accepted Manuscript



This article can be cited before page numbers have been issued, to do this please use: J. Faivre, G. Sudre, A. Montembault, S. Benayoun, X. Banquy, T. Delair and L. David, *Soft Matter*, 2018, DOI: 10.1039/C8SM00215K.



This is an Accepted Manuscript, which has been through the Royal Society of Chemistry peer review process and has been accepted for publication.

Accepted Manuscripts are published online shortly after acceptance, before technical editing, formatting and proof reading. Using this free service, authors can make their results available to the community, in citable form, before we publish the edited article. We will replace this Accepted Manuscript with the edited and formatted Advance Article as soon as it is available.

You can find more information about Accepted Manuscripts in the [author guidelines](#).

Please note that technical editing may introduce minor changes to the text and/or graphics, which may alter content. The journal's standard [Terms & Conditions](#) and the ethical guidelines, outlined in our [author and reviewer resource centre](#), still apply. In no event shall the Royal Society of Chemistry be held responsible for any errors or omissions in this Accepted Manuscript or any consequences arising from the use of any information it contains.

Article type: Full Paper

Bioinspired Microstructures of Chitosan Hydrogel Provide Enhanced Wear Protection

Jimmy Faivre, Guillaume Sudre, Alexandra Montembault, Stéphane Benayoun, Xavier Banquy, Thierry Delair, Laurent David**

J. Faivre, G. Sudre, A. Montembault, Prof. T. Delair, Prof. L. David

Université de Lyon, Université Claude Bernard Lyon 1, CNRS, IMP, UMR 5223, 15
Boulevard Latarjet, F-69622, Villeurbanne, France

*E-mail: laurent.david@univ-lyon1.fr

J. Faivre, Prof. X. Banquy

Canadian Research Chair in Bioinspired Materials, Faculty of Pharmacy, Université de
Montréal, Montréal, Qc, Canada

*E-mail: xavier.banquy@umontreal.ca

Prof. S. Benayoun

Laboratoire de Tribologie et Dynamique des Systèmes, UMR 5513 CNRS, Ecole Centrale de
Lyon, 36 Avenue Guy de Collongue, 69134 Ecully Cedex, France

[Abstract]

We describe the fabrication of physical chitosan hydrogels exhibiting a layered structure. This bilayered structure, as shown by SEM and confocal microscopy, is composed of a thin dense superficial zone (SZ), covering a deeper zone (DZ) containing microchannels orientated perpendicularly to the SZ. We show that such structure favors diffusion of macromolecules within the hydrogel matrix up to a critical pressure, σ_c , above which channels were constricted. Moreover, we found that the SZ provided a higher wear resistance than the DZ which was severely damaged at a pressure equal to the elastic modulus of the gel. The coefficient of friction (CoF) of the SZ remained independent of the applied load with $\mu_{SZ} = 0.38 \pm 0.02$, while CoF measured at DZ exhibited two regimes: an initial CoF close to the value found on the SZ, and a CoF that decreased to $\mu_{DZ} = 0.18 \pm 0.01$ at pressures higher than the critical pressure σ_c . Overall, our results show that internal structuring is a promising avenue in controlling and improving the wear resistance of soft materials such as hydrogels.

1. Introduction

Hydrogels scaffolds are receiving a growing interest in tissue engineering since they can advantageously combine cytocompatible polymers with a high amount of water, therefore, mimicking living tissues¹. These materials have been used as scaffolds for cartilage^{2,3}, bone⁴, or nervous tissue repair⁵. In addition, they can be used as artificial skin^{6,7}, or as carriers for drug delivery of active molecules⁸⁻¹⁰. These applications emerge from their tunable chemical properties, their multi-scale microstructure (porosity, crystallinity, macromolecular network topology), and their adjustable mechanical and physical properties (viscoelasticity, toughness, permeability^{11,12}).

The design of tissue-mimicking hydrogels for a specific application depends on the choice of raw material (natural polymers or biocompatible synthetic polymers) and the gelation technique. A useful concept for hydrogel design is bio-inspiration: to take advantage of naturally-occurring chemical and physical architectures for manipulating physical, mechanical and biological behaviors^{13,14}. This material development strategy leads to the concept of hydrogel materials as “decoys for biological media”³. The methods used to induce structuring within hydrogels at different length scales are themselves of great interest. The common structuring methods include freeze or vacuum-casting, layer-by-layer deposition, templating, 3D-printing, and self-assembly, which are used depending on the polymer nature and/or the solvent^{13,15}. Despite the significant number of reports demonstrating the intimate relationship between hydrogels microstructure and macroscopic properties, very few reports have focused on the control of the tribological properties, especially wear resistance. This lack of fundamental knowledge has hampered the use of structured hydrogels in many biomedical applications such as joint replacement. In the present study, we demonstrate that the generation of bioinspired microstructures in physical chitosan hydrogels dramatically allows

to control their lubrication and wear resistance. Chitosan hydrogels are especially suitable for cartilage repair since they are excellent for 3D-chondrocyte growth and proliferation^{2, 3, 16}, and for cartilage substitutes^{17, 18}. In this paper, we focus on the impact of the hydrogel structuring on their transport and mechanical properties and more specifically on hydrogel/hydrogel tribological properties to understand and rationalize the effects of the multi-scale structure on wear resistance.

2. Results

2.1 Structure of chitosan hydrogels

The "one-pot" fabrication process (see Experimental Section) facilitates the manufacturing of chitosan physical gels with controlled architecture (Fig. 1). The process allows obtaining a two-layered structure as depicted in figure schematic 1A. During the gelation process, the

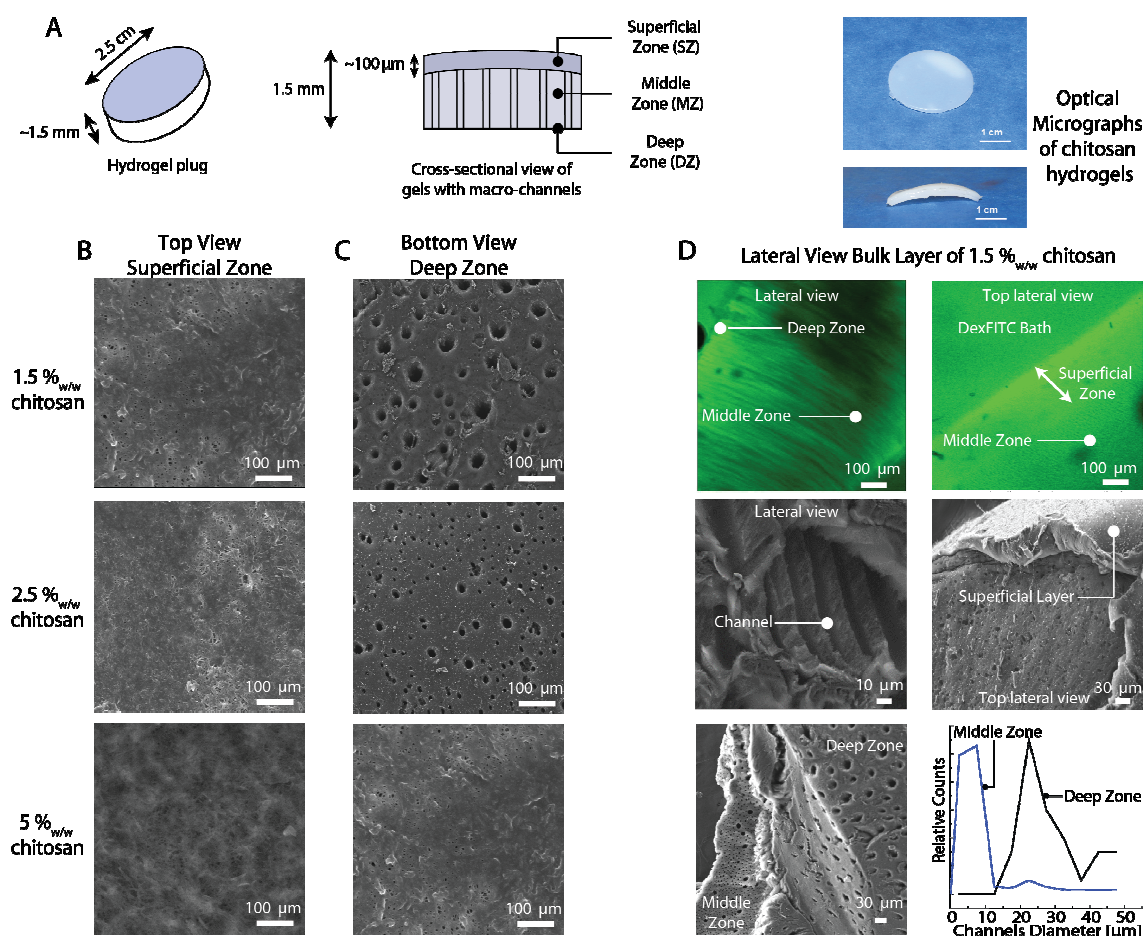


Figure 1. Structural understanding of physical chitosan hydrogels. (A) Scheme of gel disk, cross-sectional view of chitosan gels owning or not macro-channels, and optical micrographs of hydrogel disks. SEM pictures of chitosan hydrogels after CO₂ supercritical drying as a function of chitosan concentration showing (B) the superficial zone (top view) exhibiting a dense structure and (C) the deep zone (bottom view) of hydrogels showing macro-porosity. (D) CLSM and SEM pictures of a cross-section of 1.5 %_{w/w} chitosan gel showing aligned channels perpendicularly to superficial zone. 40 kDa Dextran-FITC was added to the gel solution to visualize the gel structure by CLSM.

acidic chitosan solution in direct contact with the basic solution quickly forms a dense gel membrane¹⁹ forming the superficial zone (SZ) of the gel (Fig 1B). Directly following the formation of the SZ, the middle zone (MZ) of the gel exhibits perpendicularly aligned channels (capillaries) of 10-25 μm in diameter (Fig. 1 C-D) depending on the gel concentration. These channels were found to be densely packed throughout the gel thickness from the upper part of the MZ down to the deep zone (DZ) (Fig 1C). The size of the channels decreased with increasing chitosan concentration, C_p , from 20 μm at 1.5 %_{w/w} chitosan gel to 10 μm for 2.5 %_{w/w} chitosan gel and no apparent channels were observed in the 5 %_{w/w} chitosan gel (Fig. 1C). To gain more insights on the structure of the bilayered hydrogel, vertical slices of 1.5 %_{w/w} chitosan gel, parallel to the channels, were imaged by confocal microscopy and SEM (Fig. 1D). The MZ exhibits vertically aligned channels while the SZ appeared as a dense layer of about 100 μm in thickness. Throughout the MZ and DZ, the distribution of the channel diameters was bimodal (Fig. 1D). In the vicinity of the membrane (upper region of the MZ), a majority of 5 μm channels and few 20 μm channels were observed. In deeper regions (DZ), the channels appeared larger with a diameter ranging between 20 and 40 μm . At a finer size scale, in order to measure the nanoporosity of the gels, we quantified the diffusion coefficient of dextran-FITC probes embedded in the gel by fluorescent recovery after photobleaching (FRAP). When the probe size is close to the mesh size of the gel or internal gel porosity, its diffusion is expected to be significantly lowered (see the fluorescent probes sizes in table S1). The mesh size for 1.5 %_{w/w} and 2.5 %_{w/w} chitosan gels were measured in the SZ and MZ and they ranged between 40 and 80 nm while the porosity of the 5 %_{w/w} hydrogels ranged between 10 and 40 nm (Fig. S1).

2.2 Poroelastic properties of structured chitosan hydrogels

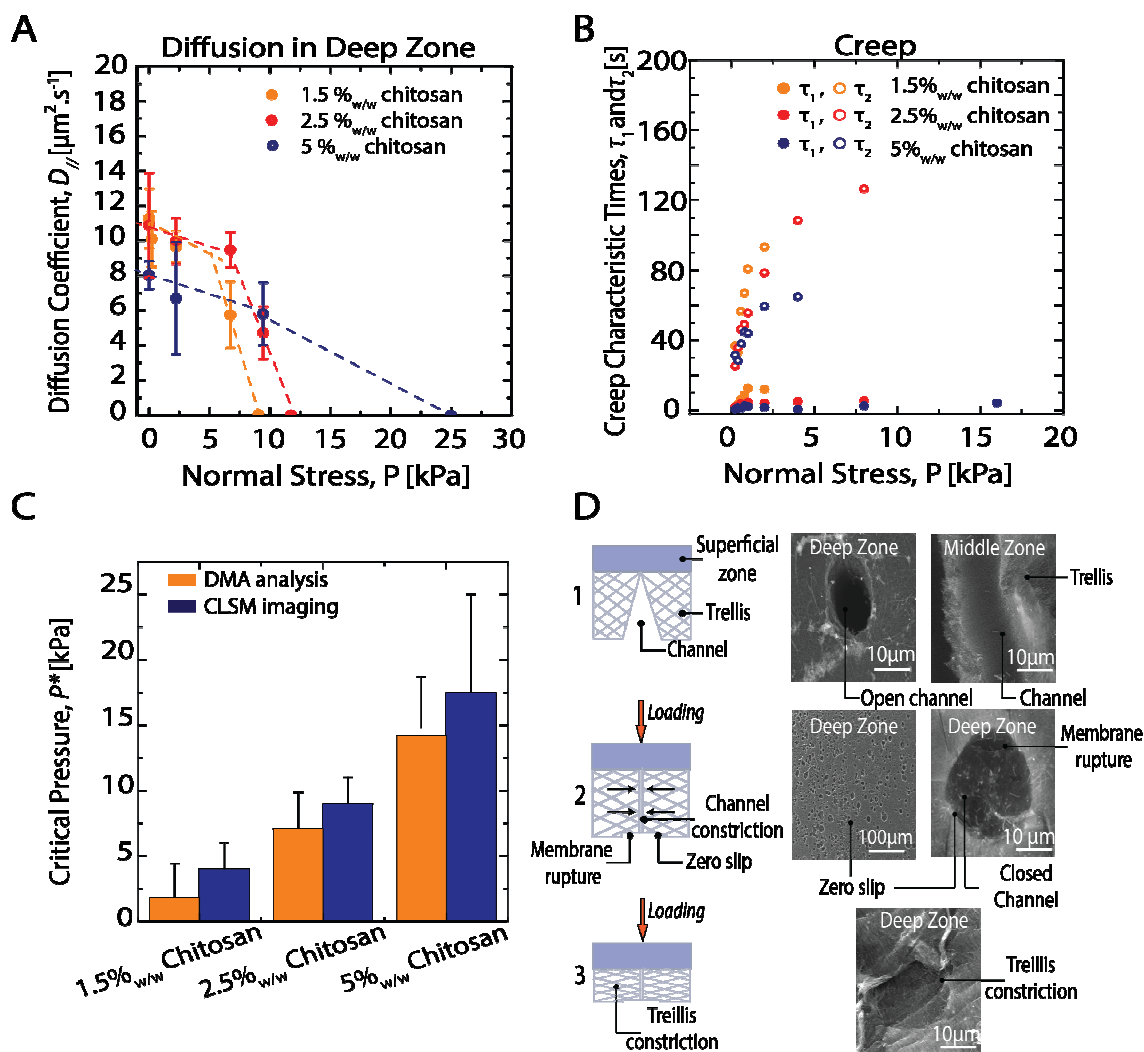


Figure 2. (A) Diffusion coefficients of 40kDa Dextran-FITC embedded in chitosan gels as a function of normal stress (error bars represents standard deviations of $n=5$ independent measurements). (B) Characteristic creep times, τ_1 and τ_2 , as a function of applied normal. (C) Comparison of the gel critical pressure, σ_c , between Dynamic Mechanical Analysis and Confocal Laser Scanning Microscopy. (D) Schematic and SEM micrographs of 2.5%_{w/w} chitosan hydrogel nano- and micro- porosity (basal view) evolution under stress: (D1) unloaded gel with open channel and normal trellis-like structure, (D2) normally loaded gel ($\sigma = 5$ kPa) showing channel constriction, and (D3) normally loaded gel ($\sigma = 50$ kPa) showing channel and trellis constriction.

To gain more insight into the fluid transport properties inside the gels under normal stress, we performed a series of FRAP experiments at different applied normal loads. A normal load was applied by depositing a weight on top of the gel immersed in a 40 kDa dextran-FITC fluorescent buffer.

At rest (no load, $\sigma = 0$), the diffusion coefficients of 40 kDa dextran probes were $12 \mu\text{m}^2/\text{s}$ for $C_p = 1.5$ and $2.5 \text{ \%}_{\text{w/w}}$ and decreased to $8 \mu\text{m}^2/\text{s}$ for $C_p = 5 \text{ \%}_{\text{w/w}}$ (Fig 2A). Under weak normal loading ($\sigma < \sigma_c$, σ_c being a critical stress at which diffusion within the gel matrix is drastically reduced), the diffusion coefficient was firstly weakly impacted. At $\sigma > \sigma_c$, the diffusion coefficient of the probe drastically decreased and could not be measured. The value of σ_c was estimated at the slope transition (Fig. 2A). The values were $\sigma_c = 2\text{-}8 \text{ kPa}$ for $C_p = 1.5\% \text{ w/w}$ and $\sigma_c = 8\text{-}10 \text{ kPa}$ for $C_p = 2.5\% \text{ w/w}$ chitosan gels. The transition was much smoother for $C_p = 5\% \text{ w/w}$ chitosan gels which complicated the determination of σ_c (estimated between $10 - 25 \text{ kPa}$).

To characterize the mechanical behavior of the structured gels, we performed creep/recovery tests at increasing normal stress on fully immersed chitosan gels using Dynamic Mechanical Analyzer (DMA) (Fig. 2B and Fig. S2A). This study allows to measure the characteristic times for creep and recovery at different loads. Initially, at $\sigma < \sigma_c'$ (σ_c' being a critical stress at which the gels does not fully recover or reach the steady state after an applied strain), the gels exhibited full elastic creep and recovery after addition and release of the normal pressure. Above σ_c' ($\sigma_c' = 1.8 \text{ kPa}$ for $C_p = 1.5 \text{ \%}_{\text{w/w}}$, $\sigma_c' = 7.1 \text{ kPa}$, for $C_p = 2.5 \text{ \%}_{\text{w/w}}$, and, $\sigma_c' = 14.2 \text{ kPa}$ for $C_p = 5 \text{ \%}_{\text{w/w}}$), gels were not able to reach the steady creep regime or recover completely (Fig. S2A). This first observation showed that $\sigma_c \sim \sigma_c'$ for all the gels tested indicating a strong correlation between the mechanical and transport properties of these gels (Fig 2C). The creep/recovery responses were fitted using the Voigt model for creep:

$$\varepsilon(t) = \varepsilon_{\text{elast}} + \sum_i \varepsilon_{ci} \left(1 - \exp\left(-\frac{t}{\tau_{ci}}\right)\right) \quad \text{Eq.1}$$

where $\varepsilon(t)$, $\varepsilon_{\text{elast}}$, ε_{ci} , are the gel deformation with time, the initial gel thickness and the gel thickness at i^{th} creep step, respectively, and τ_{ci} , is the characteristic time of the i^{th} creep step.

Concerning the recovery process, at $\sigma=0$:

$$\varepsilon(t) = \varepsilon_{\infty} + \sum_i \varepsilon_{ri} \left(1 - \exp\left(-\frac{t}{\tau_{ri}}\right)\right) \quad \text{Eq. 2}$$

where ε_{∞} is the non-recoverable deformation at the end of the recovery step, ε_{ri} is the amplitude of the i^{th} recovery component, and τ_{ri} is the characteristic time of the i^{th} recovery component.

In practice, two exponential terms were sufficient to adequately describe both the creep and recovery responses ($i = 2$), yielding to two characteristic times for creep, τ_{c1} and τ_{c2} , and recovery, τ_{r1} and τ_{r2} , and their corresponding amplitudes. Thus, these observations evidenced two different deformation regimes. A first process occurred with a characteristic time τ_{c1} and τ_{r1} of about 5-10 s for creep and recovery, independently of chitosan concentration (full symbols in Fig 2B and Fig. S2B). During this first stage, at least 95% of the gel thickness deformation occurred at $\sigma < \sigma_c$. This was followed by a slower process with a characteristic time τ_{c2} and τ_{r2} , ranging from 30 to 100 s, responsible for less than 5% of the gel deformation (in the investigated creep and recovery time ranges).

To understand the nature of these 2 distinct deformation regimes, 1.5%_{w/w} chitosan gels were imaged by SEM at $\sigma < \sigma_c$ (Fig. 2D1), at $\sigma > \sigma_c$ (Fig. 2D2), and $\sigma \gg \sigma_c$ (Fig. 2D3). At $\sigma < \sigma_c$, the initial gel structure was not affected by the applied normal stress. The hydrogel still exhibited open pores and channels. At $\sigma > \sigma_c$, the channels were fully filled with the polymer matrix. The opening of the pores in the DZ were still noticeable due to the adhesion of the gel to the glass substrate during sample preparation for SEM (creating a zero slip boundary). At $\sigma \gg \sigma_c$, the nanoporosity collapsed leading to the closure of the nanoporosity, referred to as “treillis constriction” in Figure 2D3.

Finally, the mechanical properties of chitosan hydrogels were assessed by a tensile tester in compression mode. Figure S3 displays a typical loading/unloading true stress-strain curve ($\sigma_v - \varepsilon_v$ curve). All gels appeared to exhibit a highly dissipative behavior characterized by a pronounced hysteretic loop. The dissipation ratio, defined as the ratio of the area under the hysteretic loop to the stress-strain tensile curve, reached values close to 1 above $\varepsilon_v = 50\%$,

which is indicative of a plastic behavior with no strain or stress recovery. At lower strain, $\varepsilon_v < 20$ to 50%, recovery was still observed (Fig. S3). We noticed that the plastic behavior of the gels appeared at stresses close to σ_c for each gel, indicating a close relationship between the water expulsion and irreversible polymer chain rearrangements in the hydrogel structure.

2.3. Tribological properties of chitosan hydrogels

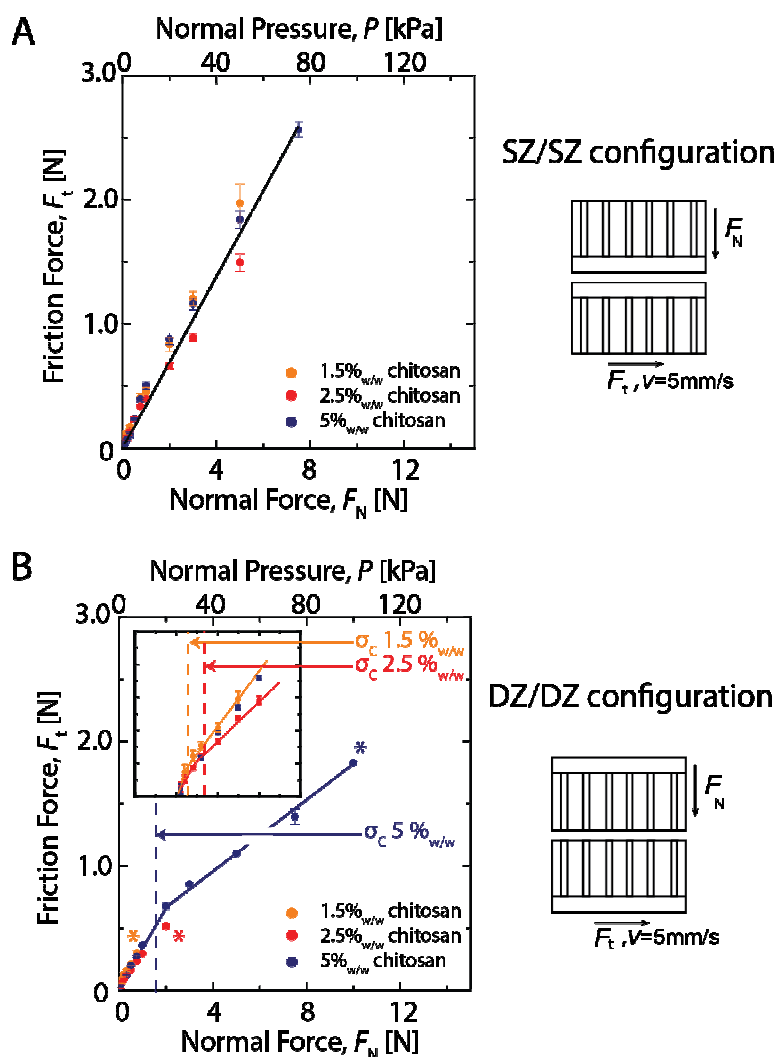


Figure 3. (A) Schemes representing the contact configurations used in the friction experiments (SZ/SZ and DZ/DZ). Friction force, F_t , as a function of normal force, F_N , (B) SZ/SZ contact and (C) DZ/DZ contact measured by low-load tribometer. * highlights the pressure at which damage occurs in the DZ/DZ configuration.

To establish the relationship between the gel microstructure and the lubrication and wear resistance, we performed a series of tribotests at different loads using two hydrogels plugs as

tribo pair. Gel/gel tribological measurements were performed in a geometry of contact plane/plane on a homemade tribometer in both SZ/SZ and DZ/DZ configurations (Fig. 3). No adhesion between the hydrogels nor stiction spikes were measured throughout the tribological experiments as shown in figure S5. Figure 3 represents the tangential force, F_t , as a function of applied normal force, F_N , at a constant sliding velocity of 5 mm/s. The gels were immersed in HEPES buffer at pH 7.4. In the configuration where the two SZ were facing each other, the Amontons coefficient of friction (CoF), μ , was $\mu = 0.38 \pm 0.02$, independently of the gel concentration (Fig 3A). When the configuration was changed to DZ/DZ configuration (Fig 3B), the measured CoF at low load was firstly very close to the SZ/SZ configuration, and reached a lower value of $\mu = 0.18 \pm 0.01$ at $\sigma > \sigma_c$, about half the SZ/SZ CoF value. Moreover, we noticed that experiments performed in the DZ/DZ configuration presented severe damage at normal pressures close to the elastic compression modulus, G' , of each gel (Fig. S4 A-B). For comparison purposes, the elastic moduli measured for the present chitosan physical hydrogels were $G' = 10$ kPa for $C_p = 1.5$ %_{w/w}, $G' = 30$ kPa for $C_p = 2.5$ %_{w/w}, and $G' = 100$ kPa for $C_p = 5$ %_{w/w} (See Experimental section in SI and Fig. S4 B). Such severe damage was *never* observed in the SZ/SZ configuration.

The lubrication and transport of lubricant/solvent between the contact zone and the bulk hydrogel were analyzed in the framework of the repulsion-adsorption model^{20, 21}.

Accordingly, the friction force of a gel on a solid substrate was written as:

$$F_t = \frac{\eta \cdot v}{\xi_g + \sqrt{K_{gel}}} \quad \text{Eq.3}$$

where v is the sliding speed, η is the viscosity of the lubricant film of thickness ξ_g , and K_{gel} is the permeability of the hydrogel to the lubricant. Upon loading and shear, the gel is excreting a thin film of lubricant maintaining the surfaces apart. Derived expressions can be used to scale the impact of the gel interfacial properties (Eq. 4)²⁰, in order to extract the interfacial fluid viscosity:

$$F_t \cong \eta \cdot v \cdot \left(\frac{E}{T}\right)^{1/3} \cdot \frac{\frac{\sigma}{E}}{1 + \frac{\frac{\sigma}{E}}{\left(1 + \frac{\sigma}{E}\right)^{1/3}}} \quad \text{Eq. 4}$$

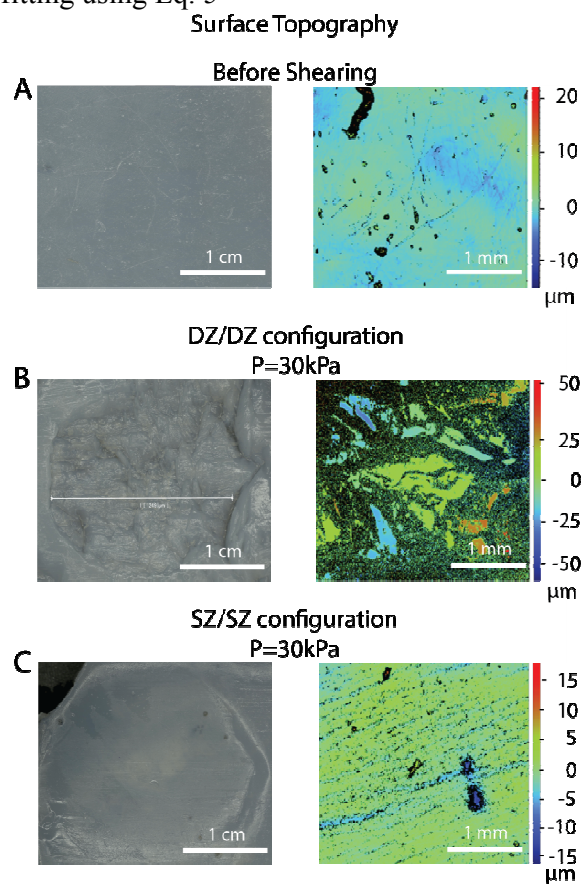
where σ is the normal pressure. The Poisson's ratio was assumed to be close to 0.5, and therefore, the elastic modulus, E , was close to $3 \times G$. For example, the 1.5 %_{w/w} chitosan gel owned a shear modulus $G = 10$ kPa, its elastic modulus was assumed to be $E = 3 \times G = 3 \times 10 = 30$ kPa. Equation 3 can also be derived to equation 5 substituting the gel permeability, yielding:

$$F_t = \frac{\eta \cdot v}{\xi \cdot \left(1 + \frac{\Pi_0}{\sigma}\right)} \quad \text{Eq. 5}$$

where Π_0 is the gel osmotic pressure and $\xi \cong \sqrt{K_{gel}}$ is the correlation length of the polymer solution. Analysis of friction data in figure 3 with equations 4 and 5 showed good agreement with the repulsive gel on solid substrate model for both configurations (Fig. S6 A-B). The viscosity of the hydrodynamic lubrication film for the DZ/DZ configuration was $\eta = 0.8$ to 1.7 mPa.s which is close to water viscosity (table 1). In the SZ/SZ configuration, η was close ranging from $\eta = 0.9$ to 2.4 mPa.s. It is noteworthy that the viscosity systematically increased when C_p decreased, suggesting a higher amount of polymer chains within the interfacial hydrodynamic film. The values of gel permeabilities, K_{gel} , in the DZ/DZ configuration were significantly higher than SZ/SZ and decreased with increasing C_p (table 1). To give more insights in the lubrication process related to a higher gel permeability, compression studies on the chitosan gels were performed. Water exudation was systematically observed on the DZ side (See video file in SI) and appeared at pressures very close to the critical pressures, σ_c , previously discussed (SI 7 ad Fig. 2C).

Table 1. Mechanical and thermodynamic properties of chitosan gel and fitted results using equation 4 and 5.

System	Elastic Modulus (Pa) ^a	Interstitial film viscosity, η		Permeability of the gel, K_{gel} (m ²) ^c	
		(mPa.s) ^b		DZ/DZ $\times 10^{-12}$	SZ/SZ $\times 10^{-12}$
		DZ/DZ	SZ/SZ		
1.5 % _{w/w} chitosan	3×10^4	1.7	2.4	10.56 (± 0.38)	2.96 (± 0.21)
2.5 % _{w/w} chitosan	9×10^4	1.0	1.8	4.53 (± 0.01)	0.76 (± 0.44)
5 % _{w/w} chitosan	3×10^5	0.8	0.9	1.80 (± 0.05)	0.15 (± 0.04)

^a fitting using Eq. 4; ^b fitting using Eq. 5**Figure 4.** 2.5%_{w/w} chitosan gel wear pictures taken by a digital microscope and using an interferometer. The gel surface is slightly dried to make streaks or fractures appear. (A) Intact gel before wear experiment, gel wear pictures in a (B) DZ/DZ configuration at 100% G' ($P = 30$ kPa) showing gel destruction, and (C) SZ/SZ configuration at 100% G' showing few damage. The black areas are due to large changes in heights. As a consequence, wear is so high that the interferometric method is unable to measure accurately the actual roughness.

We analyzed the surface topography of the 2.5 %_{w/w} chitosan hydrogels after tribotesting to assess their resistance to wear. Figure 4 shows 2.5 %_{w/w} chitosan gel topography using optical

microscopy and light interferometry to quantify changes in roughness before and after tribo experiment. The initially intact gel exhibited a smooth surface (Fig. 4A). After applying a normal stress of 100% of the value of G' (~ 30 kPa) for the 2.5 %_{w/w} chitosan hydrogel, severe wear damage appeared on the DZ/DZ contact only (Fig. 4B). Wear damage was directly observable by digital microscopy *via* the presence of large variations of the surface profile in figure 4B, matching the black areas reported in the optical interferometry images. In the SZ/SZ, the gel surface demonstrated fewer signs of wear even though CoF in this configuration was higher (Fig. 4C). This could be explained by the weaker elastic compressive modulus of the DZ compared to the SZ even over 1.5 mm of gel thickness due to the gelation process¹⁹. These qualitative observations were confirmed by the quantitative assessment of surface roughness, S_a , using interferometry (Fig. 5). Figure 5 represents the surface roughness of chitosan gel samples after shearing the surface for 10^4 cycles at a normal load of 30 kPa. The values of the surface roughness obtained from interferometry followed the previous trend observed with optical microscopy. Indeed, a low increase of surface roughness on the SZ from 0.7 to 1.1 μm with the applied pressure was noticed. In contrast, a drastic increase of S_a with the DZ/DZ configuration was observed from 4 μm to higher than 12 μm due to gel erosion and fracture at $\sigma = 30$ kPa (the final roughness is a lower bound estimation of the exact value due to large variations of the surface height in the black regions in Figure 4B). In spite of the significant damage observed by microscopy imaging, the evolution of the CoF throughout the wear test was constant, meaning that tangential forces remained constant at a fixed normal force.

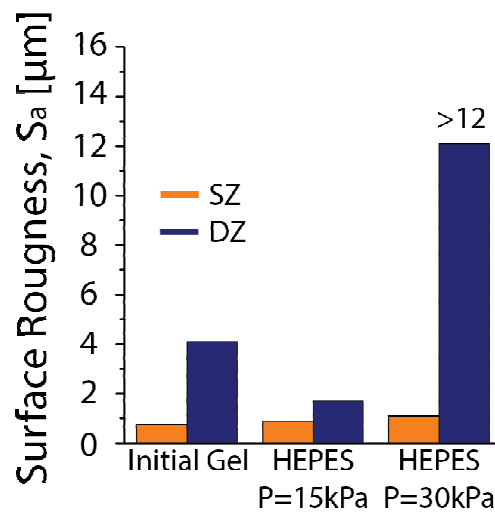


Figure 5. Quantitative analysis of gel roughness after 10^4 cycles at 5mm/s and under an applied load equals to 100% of elastic modulus of 2.5 %_{w/w} chitosan hydrogel (30 kPa) in 0.1M HEPES buffer pH 7.4. The analyzed area was 20% of the total wear track.

3. Discussions

The one-pot gelation process allowed for the formation of a structured chitosan hydrogel mimicking naturally occurring features found in cartilage^{22, 23} such as the superficial membrane (SZ) and the middle zone composed of vertically aligned channels. The formation of these microstructures is the result of a two-steps process: first, the rapid gelation of chitosan chains at the interface between the chitosan solution and the base solution and second, a slower gelation regime occurring deeper within the gel leading to partial disentanglements and formation of channels. Recent reports have shown that chitosan hydrogels exhibit such a multi-layered structure that depends on the kinetics of the gelation process^{2, 19, 24}. A similar multi-layered structure has also been reported for different natural polymer, such as collagen²⁵ and alginates²⁶.

The transport properties of the structured gels exhibit similarities to those observed in natural cartilage. The diffusion coefficient of polymeric probes obtained in our study were close to that deduced from similar experiments carried out on articular cartilage using a 70 kDa dextran-FITC fluorescent probe. Fetter *et al.* obtained a diffusion coefficient parallel to the cartilage surface of $34 \mu\text{m}^2/\text{s}$ ²⁷, while Greene *et al.* measured a diffusion coefficient of $3.8 \mu\text{m}^2/\text{s}$ ²⁸. Our results show that under normal load, the 40 kDa dextran-FITC probe diffusion in the layered gel was close to the NMR and FRAP studies from Greene *et al.*²⁸. These authors also reported a constant value of the diffusion coefficient below a critical stress and an abrupt drop of diffusion above this stress²⁸. The authors explained such behavior to result from the compression of a treillis-like structure with channels distributed vertically. Upon compression at $\sigma < \sigma_c$, the collapsing channels do not impact macromolecule diffusion inside the matrix. At higher compression (at $\sigma > \sigma_c$), the treillis constriction leads to a drastic decrease of the probe

diffusion. In our study, this phenomenon was observed at $C_p = 1.5$ and 2.5 %_{w/w} and was less pronounced for the 5 %_{w/w} chitosan gel which does not present these channels.

Our results showed that the layered microstructure of the gels lead to peculiar poroelastic properties, observed only in natural materials similarly structured.

In addition, we observed two mechanical regimes separated by a critical pressure, σ_c , which depends on C_p . At $\sigma < \sigma_c$, the gels were found to behave as viscoelastic materials with short characteristic creep and recovery times. In this regime, the porosity of the gels was not affected by the load as shown by probe diffusion measurements. Below σ_c , the channels provide enough free volume to facilitate fluid transport. Interestingly, for the gels that did not present microchannels (but still exhibited the superficial membrane), these changes in mechanical properties were still apparent around σ_c , but were less pronounced in terms of transport properties (diffusion). This observation confirms that the channel structure has a prominent role on fluid transport and polymer diffusion rather than on the mechanical properties. Above σ_c , microchannels were found to be obstructed, limiting fluid flow within the polymer matrix. Beyond this regime, the hydrogels suffered irreversible mechanical changes and plastic deformations.

The tribological behavior of the gels was not controlled by their mechanical properties since the CoF was independent of C_p for each configuration tested. At $\sigma < \sigma_c$, the CoF was independent of the configuration ($\mu \sim 0.3$), while at $\sigma > \sigma_c$, we observed that $\mu_{SZ/SZ} > \mu_{DZ/DZ}$. The observed friction change on the DZ/DZ configuration at $\sigma > \sigma_c$ is attributed to the hydrogel deformation, the microchannel closure and the water exudation to the surface leading to a more efficient lubrication. Our results show for the first time a correlation between the gel permeability and the COF suggesting that the friction dissipation at the hydrogel interface involves exudation via liquid pressurization. This is in agreement with the results of Khosla *et al.* who showed a drastic drop of CoF for porous PDMS surfaces sliding

in water due to the creation of pressurized water pockets able to feed the hydrodynamic lubrication film²⁹.

The gel wear resistance was found to be governed by the hydrogel layered-structure since the SZ/SZ configuration exhibited significantly less wear than the DZ/DZ configuration. Therefore, the gel membrane present at the SZ acts as a protective layer which mechanical and transport properties are very different from those of the gel bulk³⁰.

In a nutshell, our observations echo many studies performed of natural materials such as structured tissues. The developed chitosan gels therefore offer a unique opportunity to study and rationalize dynamic mechanical processes occurring in such tissues under controlled conditions.

4. Conclusion

The present work shows that structuring allows controlling wear and lubrication independently without the necessity of changing material or lubricant composition. Bioinspiration is thus a promising route to design efficient cartilage substitutes by taking advantage of the natural structures found in living tissues. A better attention should be paid to the transport and tribological properties of hydrogels, besides the choice of the polymer and the focus on the mechanical properties, to ensure adequate response and sustainability *in vivo*. Further studies are ongoing to improve the lubrication and anti-wear properties of soft and porous materials by using synthetic synovial fluids interacting synergistically and dynamically with such hydrogels³¹.

5. Experimental Section

5.1 Materials

Chitosan (M_w 6.04×10^5 g/mol, M_w/M_n 1.64, DA 4.3%, from squid pen chitin) was purchased from Mahtani Chitosan Pvt. Ltd. Acetic acid, ammonium hydroxide, HEPES and FITC-modified dextran probes (4.0×10^4 g/mol, 5.00×10^5 g/mol, and 2.00×10^6 g/mol) were supplied from Sigma-Aldrich. NaOH pellets, NaCl, and absolute anhydrous ethanol were obtained from Carlo Erba Reagents.

5.2 Chitosan Purification

Chitosan was purified on filtration columns with Millipore membranes. A 0.5 %_{w/w} acidic chitosan aqueous solution was prepared by adding a stoichiometric amount of acetic acid to glucosamine units. The solution was passed through filtration columns with a pressure kept constant at 3 bars with membrane porosities of successively 3, 0.8, and 0.45 μm . Chitosan was precipitated by adding a small amount of ammonium hydroxide to get a pH of 9 and thoroughly washed with distilled water using a centrifuge (10 min at 10000 rpm). Supernatant was removed and replaced by pure water and the procedure was repeated up to distilled water pH. Finally, chitosan was freeze-dried to obtain a purified powder.

5.3 Polymer Characterizations

The molar mass, dispersity, and radius of gyration of chitosan and dextran fluorescent probes were analyzed using aqueous Gel Permeation Chromatography (Wyatt Technology). Refractive Index (rEX), UV (DAWN HELEOS), and QELS (Wyatt QELS+) detectors were used for the experiments. GPC parameters for chitosan analysis were: flow rate 0.5 mL/min, $dn/dc(\text{chitosan})$ 0.198 mL/g, TSK6000 and TSK2500 columns (Tosoh Bioscience LLC.), column temperature 25 °C, laser wavelength 664 nm. Samples were dissolved at 0.5 mg/mL in filtered acetic acid buffer (pH 4.5, filtered at 0.1 μm using CME membrane) and filtered at

0.45 μm on CME membrane. For dextran-FITC analysis, parameters were: flow rate 0.5 mL/min, $dn/dc(\text{DexFITC})$ 0.152 mL/g, TSK6000 and TSK2500 columns, column temperature 25 $^{\circ}\text{C}$, laser wavelength 664 nm. Samples were dissolved at 0.5 mg/mL in filtered Phosphate Buffered Saline buffer (PBS) (pH 7.4, 10 mM PBS, 0.15 M NaCl, filtered at 0.1 μm using CME membrane) and filtered at 0.45 μm on CME membrane.

The degree of acetylation of chitosan was assessed using $^1\text{H-NMR}$ spectroscopy (Bruker 400 MHz). The DA was calculated according to the method of Hirai et al.,³² from the ratio the integration of acetyl group protons (δ : 2.4-1.7 ppm) by the integration of glucosamine unit protons (δ : 4.3-2.7 ppm). Chitosan was dissolved in D_2O with 5 μL of 37 % HCl solution for 12 h at room temperature.

5.4 Chitosan hydrogel disks

A chitosan solution was prepared by dissolving purified chitosan powder into water at the polymer concentrations 1.5, 2.5 and 5 %_{w/w} with a stoichiometric amount of glacial acetic acid to ensure the protonation of every amino groups using the following equation:

$$m_{chitosan} = \frac{m_{chitosan} \times (1 - DA) \times (1 - \frac{m_{water}}{100}) \times M_{acetic\ acid}}{M_{chitosan}} \quad \text{Eq. 6}$$

m being the mass (g), M is the molar weight (g/mol) and $M_{chitosan}$ is defined by $M_{chitosan} = 42 \times DA + 161$ ³³⁻³⁵. The chitosan dissolution was performed in a closed reactor under mechanical stirring at 4 $^{\circ}\text{C}$ for one day. The resulting chitosan solution was then placed in centrifuge syringes (Optimum®, Nordson EFD, USA) to remove air bubbles by repetitive centrifugations (5 min at 5000 rpm) and was extruded between two plastic foils with holds to control the thickness of the final gels (1.5 mm). The upper plastic foil was removed and the flattened chitosan solution was placed in a 1 M NaOH coagulation bath until the gelation process was completed. Gel disks were then cut with a biopsy punch of 11 or 25 mm diameter

and washed several times in distilled water to reach deionized water pH. The obtained hydrogel disks were stored in distilled water prior to use.

5.5 SEM on chitosan aerogels

Hydrogel samples were firstly changed for 100% alcogel by immersing hydrogels into successive ethanol baths (10, 30, 50, 70, 90, and 100% ethanol in water) for 30 min each. Aerogels were obtained by exchange between ethanol and CO₂ supercritical fluid using an automated critical point dryer (EM CPD300, Leica). 20 exchange cycles were needed followed by a very slow CO₂ degassing at 37 °C. Samples were then carbonated and imaged using an scanning electronic microscope (Merlin Compact, Zeiss). To visualize the impact of a normal stress on the gel structure, precisely weighted loads was applied on top of the hydrogels prior to aerogel formation.

5.6 Observation of hydrogels and FRAP experiments by confocal laser scanning fluorescence microscopy (CLSM)

CLSM micrographs of the hydrogels were obtained using a laser scanning confocal microscope (Zeiss 510 LCM) with a 10 x 0.3NA dry neofluor objective. Chitosan hydrogels were incubated with 0.6 mg/mL 40 kDa dextran-FITC fluorescent probes in a HEPES buffer (0.1 M HEPES, 150 mM NaCl and pH 7.4) for 24 h in a dark container at 4 °C. Excitation was conducted at 488 nm at 3% laser intensity (excitation laser source was set at 50%) and emission collected from 505 to 670 nm. The photomultiplier (PMT) gain was set at 525. Pictures were taken in a fluorescent probe bath on both sides and on the side of a gel slice. Imaging, gel porosity, and macromolecule diffusion under stress were recorded by Fluorescence Recovery After Photobleaching (FRAP) technique³⁶ at a depth of 100 μm. In each experiment, small hydrogel disks were cut from chitosan gel membranes to get 5 mm diameter and 1.5 mm thick pieces and were incubated in 0.6 mg/mL 40 kDa dextran-FITC buffered solution (0.1 M HEPES, 150 mM NaCl and pH 7.4) for 24 h to ensure complete homogenization. The gels were then mounted in CLSM and immersed in the fluorescent

probe buffered solution. For FRAP experiment under load, each dextran-FITC concentration was fixed at 0.6 mg/mL and PMT gain was kept constant at 525. To ensure the recording of a 2D diffusion (in the focal plan) and the use of a mathematical fit, a full cylinder was bleached after intense photobleaching (100% laser intensity)³⁶. In this case, the cylindrical bleaching volume avoids diffusion in the third dimension. 512x512 pixels images of a confocal xy plan (100 μm above the bottom of the plate, 15 μm of thickness) were scanned at 3 % laser initial intensity ($I < 0$) (15 pre-bleach scan images). At $t = 0$, a circle of 55 μm diameter is bleached with 50 iterations (about 10 s total) at 100 % laser intensity (I_0). A total of about 500 images scans (acquisition time < 1 s each) were collected for each sample. 5 repetitions were done per experiment. For diffusion under stress experiments, weights were deposited on a cover glass directly on top of the disks. To measure the diffusion coefficients, the gels were left to equilibrate 5 min prior to FRAP measurements. The transitory state was also recorded.

5.7 Mechanical properties by Dynamic Mechanical Analysis

Gel samples were die-cut with a 12 mm diameter punch and placed in a compression module. An aqueous bath was mounted to maintain complete hydration of gel disks and also water recovery after unconfined compression at room temperature. Firstly, a series of creep/recovery experiments were performed under constant stress using a DMA (DMA 800, TA Instrument). An initial preload of 0.02 N was applied to measure the sample thickness. Then, a constant load was applied for 5 min and the gel length was monitored as a function of time. After 5 min of gel creep, the load was removed (set to initial value of 0.02 N) and the gel was free to re-swell. The gel length recovery was then monitored as a function of time for 5 min. This cycle was repeated several times with increasing loads upon creep from 0.05 to 2 N (corresponding to stresses from 0.5 to 20 kPa). Data were fitted using the Maxwell's approach taking into account the sum of different phenomena of specific response time via a sum of exponentials.

5.8 Tribological properties

Due to the process of gelation, physical chitosan hydrogel disks offered a bilayered structure. To assess friction properties of chitosan hydrogels on both sides, die-cut gel disks were tested by putting into contact either SZ/SZ or DZ/DZ configurations. A low-load tribometer consisting of an upper mobile part applying a sinusoidal motion and a servo-controlled load (to avoid the relaxation effect of the gel) and a lower immobile part sensing the normal and lateral forces was used. A cantilever spring (linking the upper mobile part and a pin where the 11 mm diameter gel disk is glued) transmitted a vertical load to the bottom surface. A nut allowed the pin to rotate to find a flat contact between the gels. The lower immobile part was equipped with lateral and normal force sensors. The lower 25 mm diameter gel was glued within a bath mounted on top of the lower immobile part. To glue the gels on metallic lower and upper parts, gels were slightly dried on the non-studied sides and deposited on waterproof glue (Superglue 3 Power Flex, Loctite). The bath was immediately filled with 0.1 M HEPES pH 7.4 buffer and left to incubate for 1 h. Both gels were brought into slight contact to ensure flat contact and the nut was tightened. The friction force and normal forces were measured as average values in the middle of the stroke (represented by green rectangles in Fig. S5) to avoid any edge effect due to the direction and speed changes and to ensure that the dynamic friction coefficient is assessed.

5.8.1 Normal force friction test: Upper and lower gels were brought into contact. A fixed 1 Hz oscillation frequency was applied along with a 5 mm lateral motion. Normal Force was successively increased from 0.05 N to 10 N (from 500 Pa to 100 kPa). Friction runs were performed over 250 cycles for each load.

5.8.2 Wear resistance: To assess wear, only 2.5 %_{w/w} chitosan hydrogels were used at 1 Hz oscillation frequency, 5 mm lateral motion and 3 N (~ G') normal forces for 10000 cycles. At the end of the test, the hydrogels were detached from the metallic parts, slightly dried on the

studied surface using compressed air, analyzed qualitatively by a digital microscope (VHX-1000, Keyence) and quantitatively by interferometry (ContourGT-K 3D, Bruker).

Supporting Information

Supporting Information is available from the Royal Society of Chemistry Library or from the author.

Acknowledgements

XB acknowledges the financial support from CHIR (CRC and Bridge grants) and NSERC (Discovery grant). JF is grateful to the Arthritis Society (TGP-16-183) and to the French Embassy for financial supports (Frontenac scholarship). We thank Agnes Crépet (IMP) and Pierre Alcouffe (IMP) for their technical assistance in size exclusion chromatography and scanning electron microscopy, respectively. We are also indebted to Matthieu Guibert (LTDS) for the low-load tribometer design and fabrication and Thomas Malhomme (LTDS) for wear characterization by interferometer. The help of Béatrice Burdin (Centre Technologique des Microstructures) for CLSM study implementation is also acknowledged.

Conflict of Interest

The authors declare no conflict of interest

Keywords

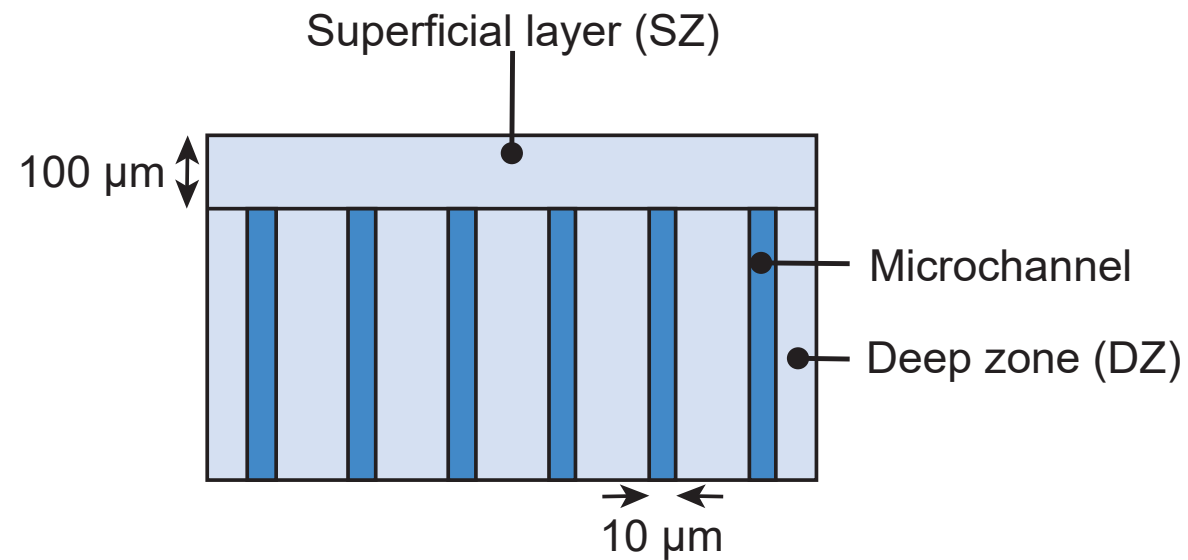
hydrogel microstructure, gel-gel friction, lubrication, wear resistance, chitosan

[References]

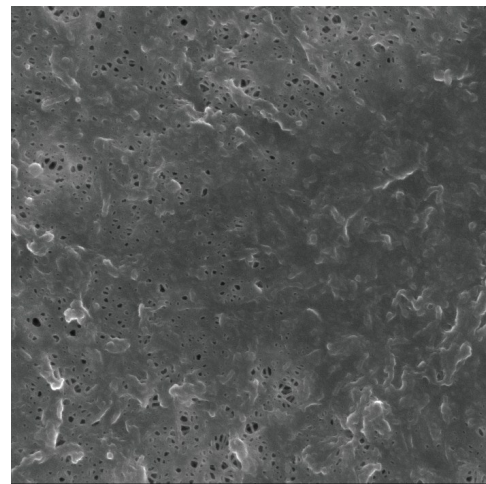
1. J. J. Green and J. H. Elisseeff, *Nature*, 2016, **540**, 386-394.
2. S. G. Ladet, K. Tahiri, A. S. Montembault, A. J. Domard and M. T. M. Corvol, *Biomaterials*, 2011, **32**, 5354-5364.
3. A. Montembault, K. Tahiri, C. Korwin-Zmijowska, X. Chevalier, M. T. Corvol and A. Domard, *Biochimie*, 2006, **88**, 551-564.
4. D. Puppi, F. Chiellini, A. M. Piras and E. Chiellini, *Progress in Polymer Science*, 2010, **35**, 403-440.
5. F.-Y. Hsieh, T.-C. Tseng and S.-h. Hsu, *Neural Regeneration Research*, 2015, **10**, 1922-1923.
6. F. Croisier and C. Jérôme, *European Polymer Journal*, 2013, **49**, 780-792.
7. J. Mao, L. Zhao, K. De Yao, Q. Shang, G. Yang and Y. Cao, *Journal of biomedical materials research. Part A*, 2003, **64**, 301-308.
8. T. R. Hoare and D. S. Kohane, *Polymer*, 2008, **49**, 1993-2007.
9. M. Hamidi, A. Azadi and P. Rafiei, *Advanced Drug Delivery Reviews*, 2008, **60**, 1638-1649.
10. P.-L. Latreille, S. Alsharif, O. Gourgas, S. F. Tehrani, V. G. Roullin and X. Banquy, *Colloids and Surfaces A: Physicochemical and Engineering Aspects*, 2017, **529**, 739-749.
11. I. M. El-Sherbiny and M. H. Yacoub, *Global Cardiology Science & Practice*, 2013, **2013**, 316-342.
12. C. A. Vilela, C. Correia, J. M. Oliveira, R. A. Sousa, J. Espregueira-Mendes and R. L. Reis, *ACS Biomaterials Science & Engineering*, 2015, **1**, 726-739.
13. S. E. Naleway, M. M. Porter, J. McKittrick and M. A. Meyers, *Advanced Materials*, 2015, **27**, 5455-5476.
14. P. Lin, R. Zhang, X. Wang, M. Cai, J. Yang, B. Yu and F. Zhou, *ACS Macro Letters*, 2016, **5**, 1191-1195.
15. M. Liu, X. Zeng, C. Ma, H. Yi, Z. Ali, X. Mou, S. Li, Y. Deng and N. He, 2017, **5**, 17014.
16. L. Rami, S. Malaise, S. Delmond, J.-C. Fricain, R. Siadous, S. Schlaubitz, E. Laurichesse, J. Amedee, A. Montembault, L. David and L. Bordenave, *Journal of Biomedical Materials Research Part A*, 2014, **102**, 3666-3676.
17. T. Hao, N. Wen, J. K. Cao, H. B. Wang, S. H. Lü, T. Liu, Q. X. Lin, C. M. Duan and C. Y. Wang, *Osteoarthritis and Cartilage*, **18**, 257-265.
18. S. Kaderli, C. Boulocher, E. Pillet, D. Watrelot-Virieux, A. L. Rougemont, T. Roger, E. Viguier, R. Gurny, L. Scapozza and O. Jordan, *International journal of pharmaceuticals*, 2015, **483**, 158-168.
19. J. Nie, W. Lu, J. Ma, L. Yang, Z. Wang, A. Qin and Q. Hu, *Scientific Reports*, 2015, **5**, 7635.
20. J. P. Gong, G. Kagata, Y. Iwasaki and Y. Osada, *Wear*, 2001, **251**, 1183-1187.
21. J. P. Gong, G. Kagata and Y. Osada, *The Journal of Physical Chemistry B*, 1999, **103**, 6007-6014.
22. I. ap Gwynn, S. Wade, M. J. Kaab, G. R. Owen and R. G. Richards, *J. Microsc.*, 2000, **197**, 159-172.
23. I. ap Gwynn, S. Wade, K. Ito and R. G. Richards, *European cells & materials*, 2002, **4**, 18-29.
24. S. Ladet, L. David and A. Domard, *Nature*, 2008, **452**, 76-79.
25. K. Furusawa, S. Sato, J.-i. Masumoto, Y. Hanazaki, Y. Maki, T. Dobashi, T. Yamamoto, A. Fukui and N. Sasaki, *Biomacromolecules*, 2012, **13**, 29-39.

26. Y. Maki, K. Ito, N. Hosoya, C. Yoneyama, K. Furusawa, T. Yamamoto, T. Dobashi, Y. Sugimoto and K. Wakabayashi, *Biomacromolecules*, 2011, **12**, 2145-2152.
27. N. L. Fetter, H. A. Leddy, F. Guilak and J. A. Nunley, *Journal of Orthopaedic Research*, 2006, **24**, 211-219.
28. G. W. Greene, B. Zappone, B. Zhao, O. Soderman, D. Topgaard, G. Rata and J. N. Israelachvili, *Biomaterials*, 2008, **29**, 4455-4462.
29. T. Khosla, J. Cremaldi, J. S. Erickson and N. S. Pesika, *ACS Applied Materials & Interfaces*, 2015, **7**, 17587-17591.
30. T. Murakami, S. Yarimitsu, N. Sakai, K. Nakashima, T. Yamaguchi, Y. Sawae and A. Suzuki, *Proceedings of the Institution of Mechanical Engineers, Part J: Journal of Engineering Tribology*, 2017, DOI: 10.1177/1350650117712881, 1350650117712881.
31. J. Faivre, B. R. Shrestha, J. Burdyska, G. Xie, F. Moldovan, T. Delair, S. Benayoun, L. David, K. Matyjaszewski and X. Banquy, *ACS Nano*, 2017, **11**, 1762-1769.
32. A. Hirai, H. Odani and A. Nakajima, *Polymer Bulletin*, 1991, **26**, 87-94.
33. N. Sereni, A. Enache, G. Sudre, A. Montembault, C. Rochas, P. Durand, M. H. Perrard, G. Bozga, J. P. Puaux, T. Delair and L. David, *Langmuir*, 2017, **33**, 12697-12707.
34. A. Fiamingo, A. Montembault, S.-E. Boitard, H. Naemetalla, O. Agbulut, T. Delair, S. P. Campana-Filho, P. Menasché and L. David, *Biomacromolecules*, 2016, **17**, 1662-1672.
35. A. Montembault, C. Viton and A. Domard, *Biomaterials*, 2005, **26**, 933-943.
36. J. C. G. Blonk, A. Don, H. Van Aalst and J. J. Birmingham, *Journal of Microscopy*, 1993, **169**, 363-374.

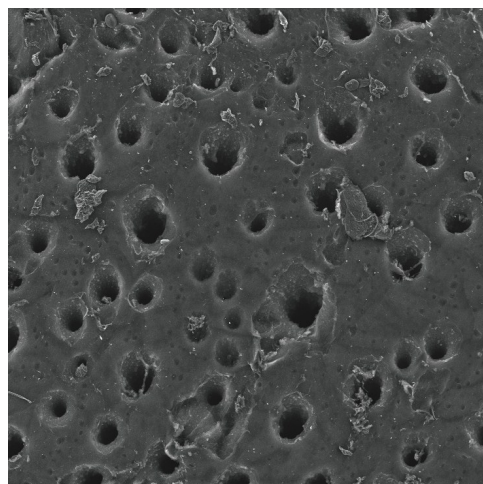
Physical Chitosan Hydrogel Structure



SEM imaging of SZ



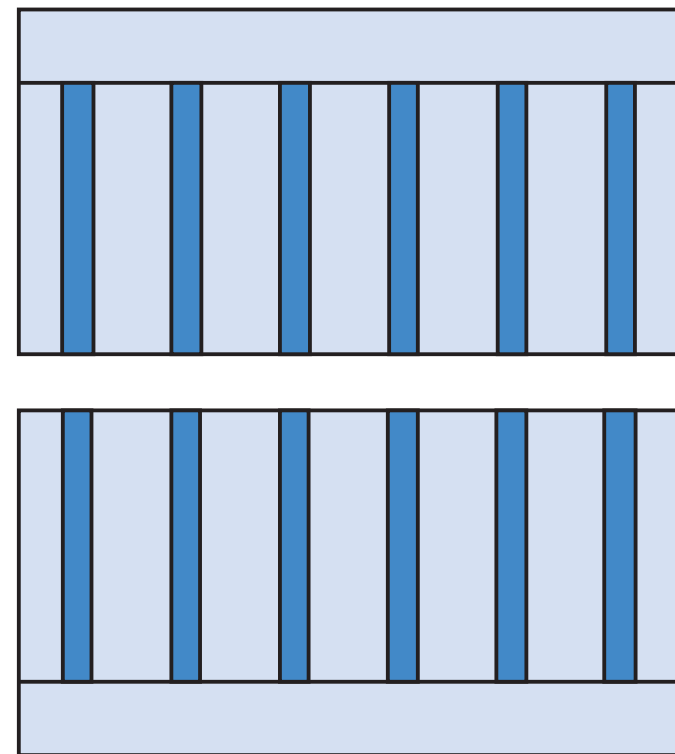
SEM imaging of DZ



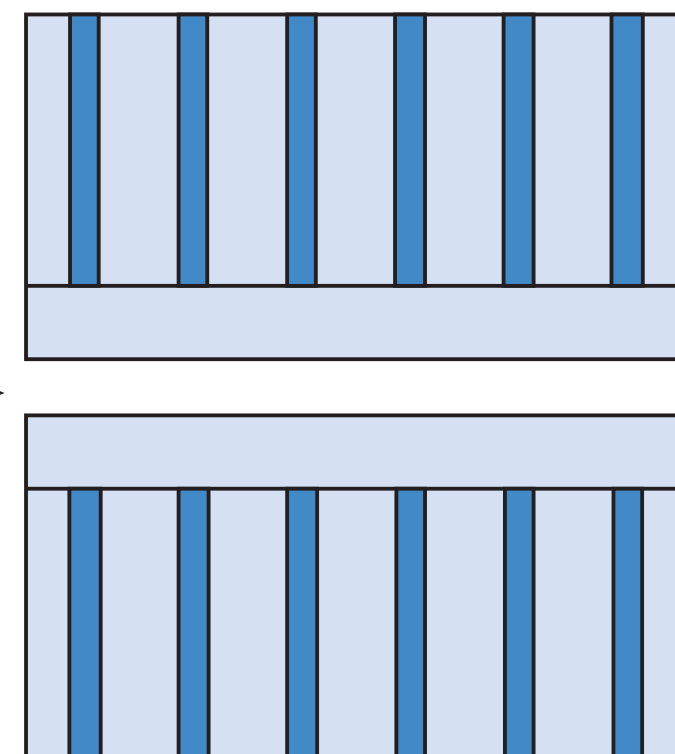
Soft Matter

DZ vs. DZ

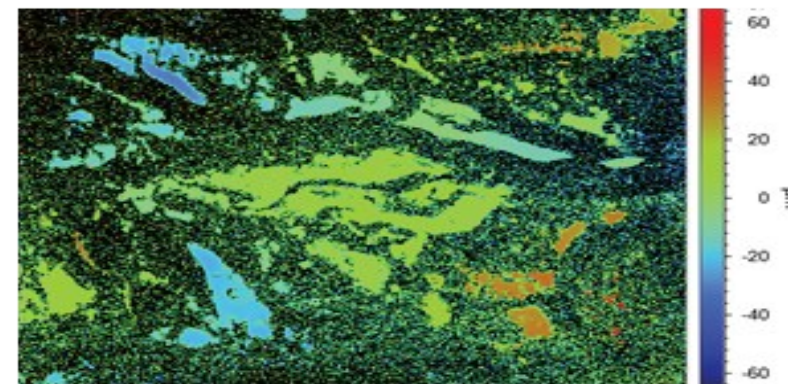
Contact Configurations for Tribo-pairs



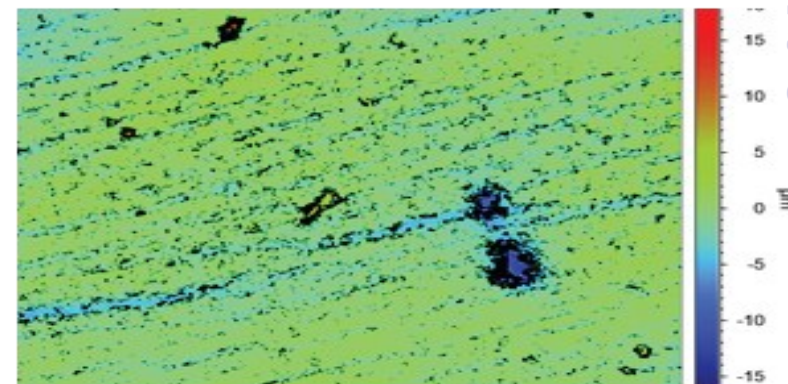
SZ vs. SZ



Wear assessment by Interferometry



$$\mu = 0.18 \pm 0.01$$



$$\mu = 0.38 \pm 0.02$$

Coefficient of Friction

Supplementary Information

Bioinspired Microstructures of Chitosan Hydrogel Provide Enhanced Wear Protection

Jimmy Faivre, Guillaume Sudre, Alexandra Montembault, Stéphane Benayoun, Xavier Banquy, Thierry Delair, Laurent David**

J. Faivre, G. Sudre, A. Montembault, Prof. T. Delair, Prof. L. David

Université de Lyon, Université Claude Bernard Lyon 1, CNRS, IMP, UMR 5223, 15
Boulevard Latarjet, F-69622, Villeurbanne, France

*E-mail: laurent.david@univ-lyon1.fr

J. Faivre, Prof. X. Banquy

Canadian Research Chair in Bioinspired Materials, Faculty of Pharmacy, Université de Montréal,
Montréal, Qc, Canada

*E-mail: xavier.banquy@umontreal.ca

Prof. S. Benayoun

Laboratoire de Tribologie et Dynamique des Systèmes, UMR 5513 CNRS, Ecole Centrale de Lyon, 36
Avenue Guy de Collongue, 69134 Ecully Cedex, France

1. Experimental Section

1.1 Rheological characterization

Chitosan hydrogel disks were characterized for their rheological properties using an AR2000 rheometer (TA Instruments, USA). A parallel plate geometry was mounted with a water trap to limit water evaporation during measurement. Viscoelastic properties were performed at 1% gel deformation in frequency sweep mode in the linear domain ($n = 5$).

1.2 Stress-strain curves

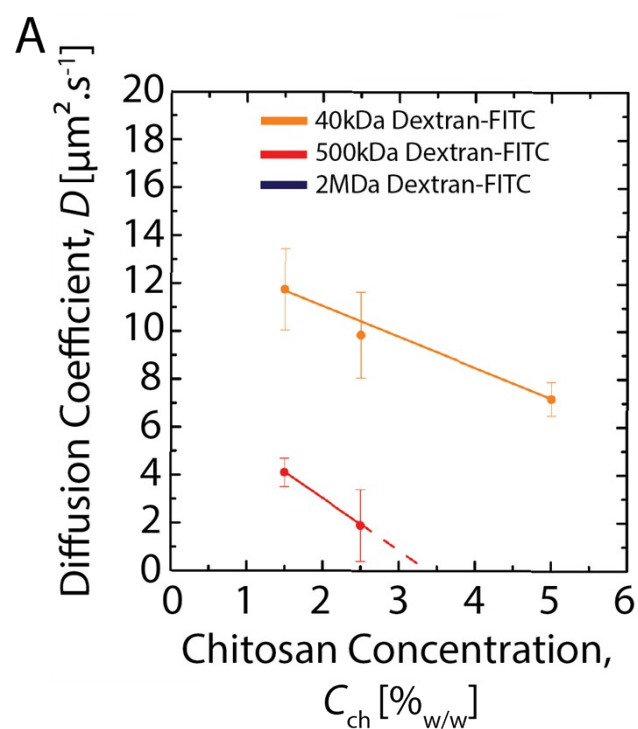
Stress-strain curves were recorded for each gel using a Shimadzu AG-X+ 10 kN tensile tester. Load/Unload cycles were applied on top of a gel with increasing strain (10, 20, 30, 50, 70, and 80% of initial gel thickness) and the resulting stress is recorded. The compression plates were lubricated with mineral oil to avoid barreling effects. A compression study was performed following the same procedure as for the stress-strain curve except that a linear strain at a rate of 0.6 mm/min was applied on top of the gels. Water exudation was directly observed by the means of a camera.

1.3 Osmotic pressure assessments

Chitosan gel osmotic pressure was evaluated to determine the gel permeability using Eq. 5. The gel osmotic pressure determinations were carried out after de-swelling the gels by the dialysis bag method described elsewhere^{1, 2}. The gel disks were positioned at the contact of semi permeable regenerated cellulose membranes (MWCO 2 kDa, spectrum lab) and the sealed bags were immersed in an aqueous polyvinylpyrrolidone solution ($8.7 \cdot 10^{-2}$ mg/mL, $M_w = 29$ kDa, Sigma-Aldrich) with a known osmotic pressure equal to 30.5 kPa and buffered with HEPES at 0.1 M and pH 7.4 at constant room temperature. After equilibrium is reached (4 days), gels are removed, weighed and viscoelastic measurements are performed using an AR2000ex rheometer to assess the shear moduli.

2. Results

2.1 Structure of chitosan hydrogels



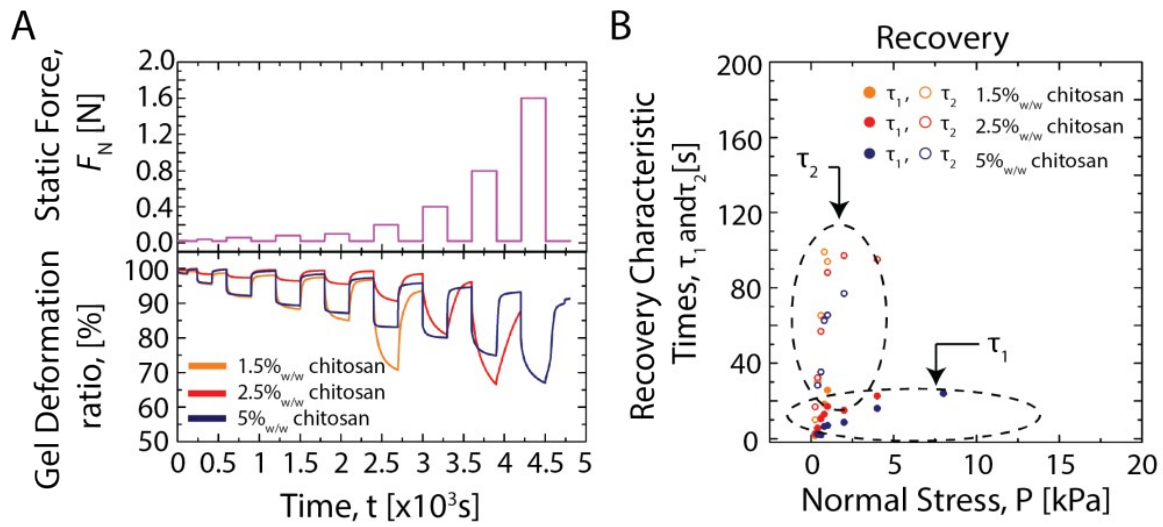
S1. Diffusion properties of chitosan hydrogels using different dextran-FITC probe sizes. 2 MDa Dextran-FITC diffusion was not detected by the FRAP technique.

Table S1. Fluorescent probe characteristics (molecular weight (Mw), dispersity (PDI) and radius of gyration (Rg)) in HEPES buffer pH 7.4 NaCl 50mM.

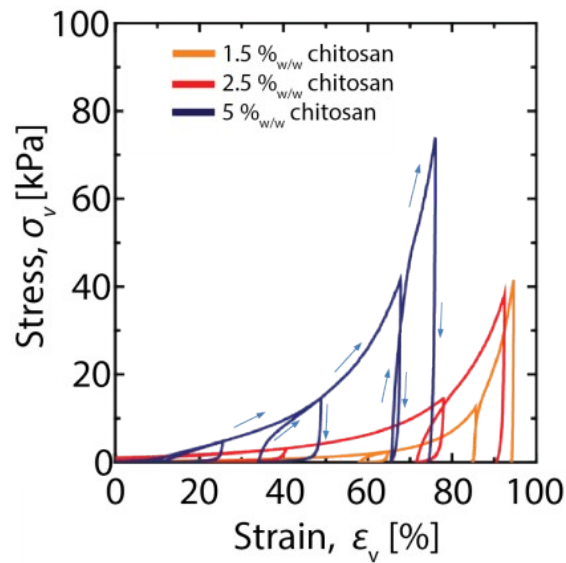
Fluorescent probe	Mw (g/mol) ^a	PDI ^a	Rg (nm) ^a	Rg (Rg=0.025*Mw ^{0.5}) ^b
40kDa DexFITC	3.85×10 ⁴	1.31	8	5
500kDa DexFITC	4.68×10 ⁵	1.81	22.5	17.7
2MDa DexFITC	1.81×10 ⁶	1.50	41.2	35.4

^a measured by GPC; ^b from literature³

2.2 Poroelastic properties of structured chitosan hydrogels

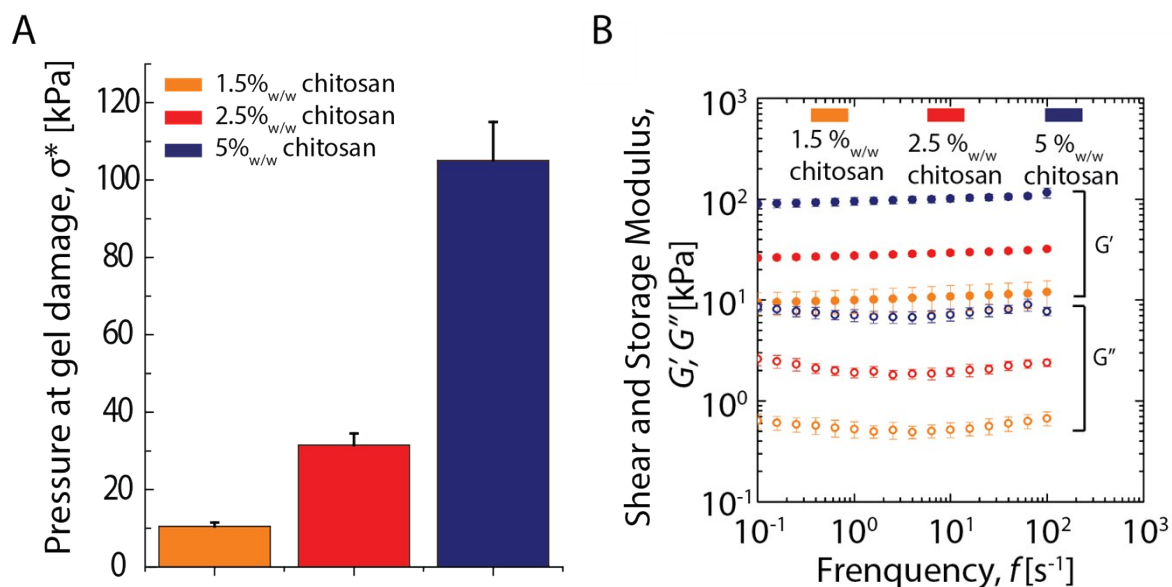


S2. (A) Creep/recovery cycles with increasing load of chitosan hydrogels assessed by DMA and (B) characteristic times of chitosan hydrogels during recovery

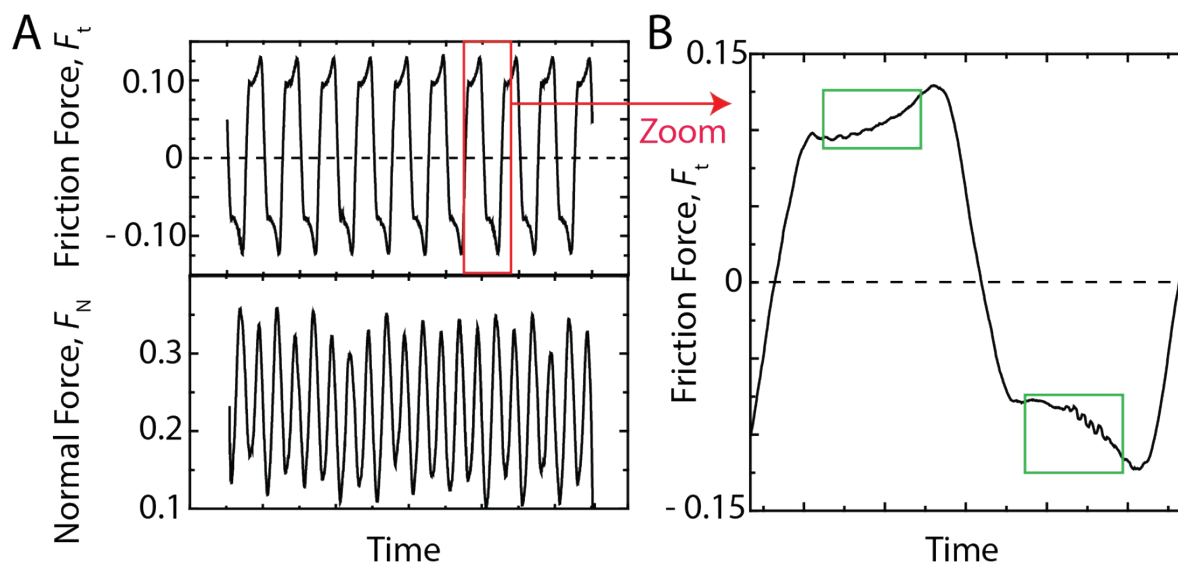


S3. stress versus strain curves of chitosan hydrogels

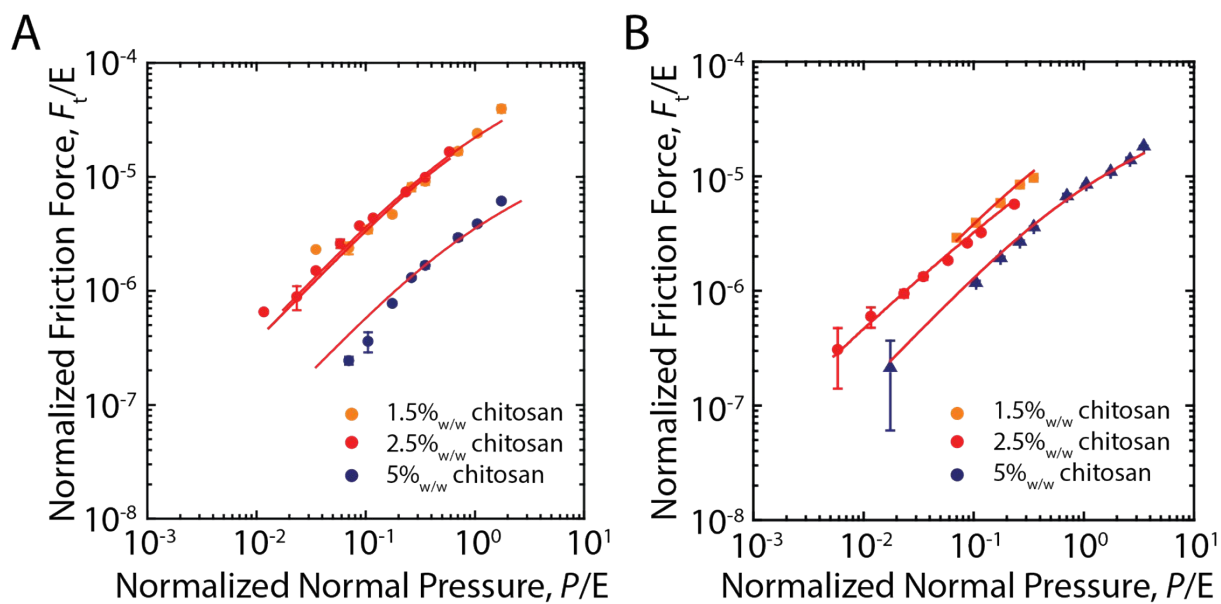
2.3. Tribological properties of chitosan hydrogels



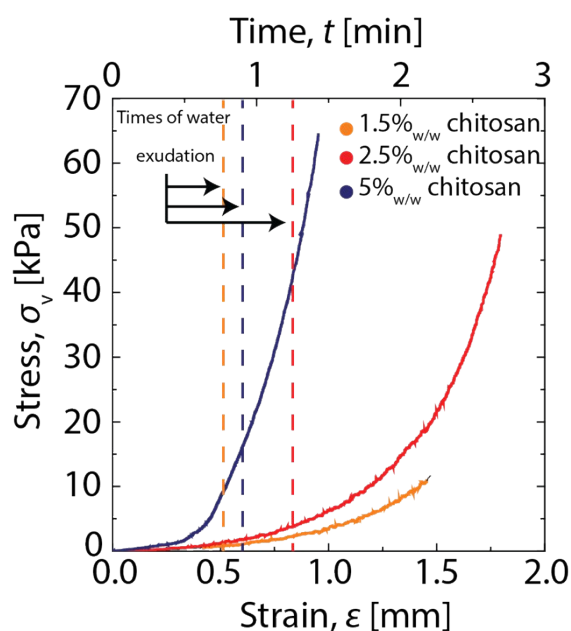
S4. (A) Pressure at gel damage measured for the chitosan hydrogels on the DZ/DZ configuration and (B) shear and storage moduli of chitosan hydrogels.



S5. (A) Typical friction and normal forces profiles for 2.5 %_{w/w} chitosan gels on the DZ/DZ configuration at a speed of $v = 5$ mm/s and (B) zoom in the friction profile showing no stiction in the friction signal. These data correspond to that of Figure 3B for the chitosan gel at 2.5 %_{w/w} at $P = 3$ kPa. Green rectangles represent the areas where the friction/normal forces were measured.



S6. Friction forces as a function of normal pressure for (A) SZ/SZ configuration and (B) DZ/DZ configuration. Red lines are fitting obtained from Eq. 1.



S7. Compression study of chitosan hydrogels showing the critical strains for exudation of water for different chitosan hydrogels.

References

1. E. Geissler, F. Horkay and A. M. Hecht, *Macromolecules*, 1991, **24**, 6006-6011.
2. F. Horkay and P. J. Basser, *Journal of polymer science. Part B, Polymer physics*, 2008, **46**, 2803-2810.
3. K. Andrieux, P. Lesieur, S. Lesieur, M. Ollivon and C. Grabielle-Madlont, *Analytical Chemistry*, 2002, **74**, 5217-5226.